Hindawi
Advances in Civil Engineering
Volume 2019, Article ID 6025698, 18 pages
https://doi.org/10.1155/2019/6025698

Research Article

Stability Charts for Pseudostatic Stability Analysis of 3D Homogeneous Soil Slopes Using Strength Reduction Finite Element Method

Chaowei Sun,[1] **Junrui Chai**,[2] **Bin Ma**,[1] **Tao Luo**,[1] **Ying Gao**,[1] **and Huanfeng Qiu**[3]

[1]*Shaanxi Key Laboratory of Safety and Durability of Concrete Structures, Xijing University, Xi'an 710123, China*
[2]*State Key Laboratory Base of Eco-Hydraulics Engineering in Northwest Arid Area, Xi'an University of Technology, Xi'an 710048, China*
[3]*Guiyang Engineering Corporation Limited, Power Construction Corporation of China, Guiyang 550081, China*

Correspondence should be addressed to Chaowei Sun; chao_wei_106@126.com

Received 8 May 2019; Revised 6 June 2019; Accepted 17 June 2019; Published 27 June 2019

Academic Editor: Hayri Baytan Ozmen

This paper uses the modified strength reduction finite element method to propose stability charts for pseudostatic stability analysis of three-dimensional (3D) homogeneous soil slopes subjected to seismic excitation. These charts are developed in a wide range of input parameters for purely cohesive slopes and cohesive-frictional slopes, respectively. Effect of the horizontal seismic load is approximately considered using the quasistatic approach. The stability charts allow to determine the factor of safety without any iterative procedure and identify the corresponding critical slope failure mechanism. A slope example is employed to illustrate the application and reliability of these stability charts.

1. Introduction

Stability charts provide an efficient tool for the rapid preestimate on slope stability. Several researches have proposed such charts for application in engineering practice in spite of the validity of numerous existing complicated commercial software for stability analysis of slopes. Taylor [1], based on the friction circle method, firstly developed the stability charts to obtain the factor of safety (FOS) for 2D purely cohesive (internal friction angle $\varphi = 0$; cohesion $c \neq 0$) and cohesive-frictional soil slopes (internal friction angle $\varphi > 0$; cohesion $c \neq 0$). According to the work of Taylor, a series of revised and improved stability charts have been routinely presented in the literature to avoid the iterative procedure since the stability number ($N = c/\gamma HF$) was introduced to define stability of the slope [2–4]. However, the above stability charts are only suitable for slope stability analysis under the hypothesis of two-dimensional (2D) plane strain. As pointed by Michalowski [5], this conventional assumption may lead to a conservative result of safety reserve for a slope with a well-defined extent of the failure mechanism. To account for the 3D effect on slope stability analyses, recent developments have focused on the extension of routine 2D methods to 3D cases. These can be divided into three major categories: the limit equilibrium method (LEM), the limit analysis method (LAM), and the strength reduction method (SRM).

Gens et al. [6] used the LEM to develop stability charts for 3D purely cohesive soil slopes. Using the LEM, Steward et al. [4] produced the updated stability charts based on the work of Taylor, which enables both the FOS and the corresponding type of the failure mode to be obtained with no need of any iterative procedure. Nevertheless, the accuracy of these chart solutions may be affected by the inherent limitations of 3D-LEM.

In the strict framework of LAM, Li et al. [7, 8] used the finite element bounding methods for limit analyses to determine the upper and lower bound of FOS and proposed two sets of stability charts for 3D homogeneous cohesive-frictional and purely cohesive soil slopes, respectively.

However, the typical condition of the seismic excitation effect was not considered in their study. In addition, Michalowski [5] adopted the 3D admissible rotational failure mechanism to produce chart solutions for estimation of the FOS of 3D homogeneous slopes with no need of any iterative procedure. Michalowski and Martel [9] proposed 3D stability charts for stability assessment of steep slopes under consideration of the seismic effect by combination of the kinematic theorem of limit analysis and the quasistatic approach. However, their work only emphasized the analysis of the toe-failure mode. The base-failure and face-failure modes were not taken into account, as shown in Figure 1. Based on the work of Michalowski and Martel [9], Gao et al. [10] exploited the analytical approach to derive the stability charts for 3D homogeneous slopes under both static and pseudostatic seismic loading conditions. Their charts are plotted for a range of geometric and material parameters that is wider than that presented by Michalowski [5] and Michalowski and Martel [9].

In addition to the above LEM or LAM, the strength reduction finite element method (SR-FEM) has been widely and successfully applied into stability analysis of slopes with improvements in science and technology in the past few decades. The typical numerical slope examples from the existing literature have indicated that the SR-FEM provides an effective and reliable approach to calculate the FOS and locate the critical failure surface (location and shape), as well as the distribution of stress, deformation, and progressive shear failure within the slope (e.g., [11] and [12–15]).

The objective of this paper is aimed at producing stability charts for pseudostatic stability analysis of 3D homogeneous soil slopes under the horizontal seismic condition. The proposed charts are developed based on the combination of the pseudostatic (PS) approach and SR-FEM in 3D seismic slope stability analyses. The effects of seismic excitation are represented by an equivalent static force, the magnitude of which is a product of a seismic coefficient k_h and the weight of the potential sliding mass [16]. In order to simplify the computational process, an alternative way to perform SR-FEM is used herein for slope stability analysis. These charts can be considered as an extension of the work of Li et al. [7, 8] to the typical condition of horizontal seismic excitation. Furthermore, they are applicable for both 3D homogeneous cohesive-frictional and purely cohesive soil slopes in a wider range of material and geometric parameters and also provide the corresponding type of the failure mode.

2. Strength Reduction Finite Element Method and Validation

2.1. Strength Reduction Finite Element Method. Both the natural and man-made slopes in geotechnical engineering practice have a certain value of safety reserve, but it may be destroyed by the effects of the internal and the external load. Researchers have often combined the strength reduction technique with the FEM when evaluating the safety reserve of a slope. Bishop first proposed the strength reduction technique in 1955, and it has been widely used in stability analysis of slopes according to the linear Mohr–Coulomb (M-C) failure criterion. Typically, the shear strength of soil is described by the M-C failure criterion as a function of the internal friction angle, φ, and the cohesion, c. Therefore, the factor of safety F is generally defined as follows:

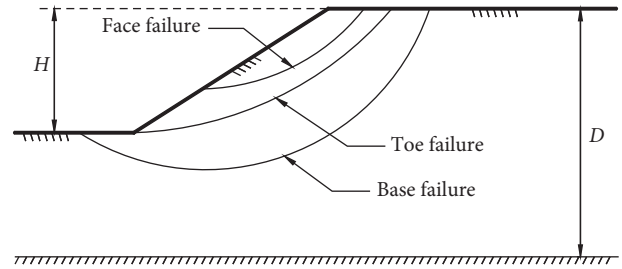

Figure 1: Three types of slope failure modes.

$$F = \frac{c}{c_f} = \frac{\tan\varphi}{\tan\varphi_f}, \tag{1}$$

where F is the reduction factor of shear strength (SRF), c and φ are the initial shear strength parameters, and c_f and φ_f are the reduced shear strength parameters.

SR-FEM is adopted to conduct the analysis for slope stability below. In the present paper, the elastic, perfectly plastic constitutive model with the M-C yield criteria is applied to the soil. Under 3D conditions, the M-C failure criterion is given as follows:

$$f(I_1, J_2, \theta) = \frac{1}{2}\left[3(1-\sin\varphi)\sin\theta + \sqrt{3}(3+\sin\varphi)\cos\theta\right] \times \sqrt{J_2} - I_1\sin\varphi - 3c\cos\varphi = 0, \tag{2}$$

where I_1 is the first stress invariant, J_2 is the second deviatory stress invariant, and θ is Lode's angle. In addition, the Drucker–Prager equation is adopted as the plastic potential function, and no tensile strength is considered. The Drucker–Prager equation is

$$g(I_1, J_2) = -\alpha I_1 + \sqrt{J_2}, \tag{3}$$

in which $\alpha = \tan\psi/\sqrt{(9 + 12\tan^2\psi)}$ and ψ is the dilation angle, which is related to the volume change in the soil while yielding. The soil is a frictional material and exhibits high dilation near the peak, eventually resulting in a residual state under the condition of a constant volume ($\psi = 0$). It is obvious that the actual volume of soil varies in the process of yielding. However, it is less important to select the soil dilation angle since slope stability analysis is relatively unconstrained [17]. Because the main purpose of this research is to determine the FOS of a slope, a compromise value of zero dilation ($\psi = 0$) during yielding is employed in this paper.

2.2. Implementation. In the SR-FEM, the conventional implementation approach of the strength reduction process is trivial because it is through modifying the input file by hand based on every SRF to do the trial calculation. In order to simplify the computational process, this paper uses an alternative way to implement the strength reduction

calculation, which was proposed by Xu et al. [18]. In strength reduction calculation, the mobilized shear strength parameters φ' and c' substitute the corresponding values of c and φ in equation (1) by the following equation:

$$c' = f(t)c,$$
$$\varphi' = \arctan[f(t)\tan\varphi], \tag{4}$$

where $f(t)$ is the field variable, $f(t) = a - bt$; t is the size of every calculation incremental step in ABAQUS, $0 \le t \le 1$; and a and b are adjustable parameters, the values of which can be set by users according to the estimation range of FOS but should meet the condition of $a/b > 1$.

Based on the work of [18], it can be found that the field variable is assigned as a function of incremental step time t, the values of c and φ can be reduced with the increase of t, and the value of SRF can be automatically obtained according to a single simulation process, which avoids modifying the input file and repeating the trial calculation. Once the reference value of the SRF is determined, it is employed for further calculations to obtain the slip surface during failure with an exhibition of a graphical output of the shear failure zone developed within the slope. In order to locate the possible slip surface, smaller incremental values of the SRF are needed in successive steps. In general, not more than ten steps are sufficient to transit to the critical limit equilibrium stage, and the shear failure zone has spread over the entire slip surface; the final FOS of a slope is obtained.

In addition, Zheng et al. [11] found and proved a so-called $\varphi - \nu$ inequality: $\sin\varphi \ge 1 - 2\nu$ (ν is Poisson's ratio). According to the inequality, ν is required to adjust as φ is reduced in strength reduction calculation so that the $\varphi - \nu$ inequality always holds. Therefore, the $\varphi - \nu$ inequality is always satisfied in the current research.

2.3. Definitions of Slope Failure. The success of SR-FEM depends largely on the global instability calculation of soil slopes, i.e., definitions of slope failure. The iteration nonconvergence of finite element numerical solution is usually considered as the global failure criterion of soil slopes [17, 19, 20]. Unfortunately, incorrect selection of the iteration method together with the incremental size may lead to initialization of the divergence of the solutions. This paper employs an alternative explicit criterion defining the slope failure. This definition of slope failure was proposed by Zheng et al. [21] and has recently received more acceptances. During the systematic reduction process for the shear strength parameters, a graphical output of the plastic shear failure zone developed within the slope is shown by the software. Slope failure occurs when the shear failure zone within the slope spreads over the entire slip surface, and the FOS is just the SRF at this state. Slope failure and nonconvergence of numerical solutions arise together and are associated with the presence of a dramatic increase in the nodal displacements within the mesh. At that time, FOS = SRF.

2.4. Boundary Conditions. It is also important to make a choice of suitable boundary conditions (BCs) when 3D slope stability analyses are conducted based on the FEM because BCs are closely related to the development of internal stress and deformation within a slope that will affect the value of the FOS together with the shape of the slip surface. Figure 2 introduces the typical 3D slope model and the BCs. The BCs for the 3D slope model can be divided into three types based on the different constraint condition of end faces: rough-rough (RR), smooth-smooth (SS), rough-smooth (RS). The explanation and applicable conditions are illustrated in Sun et al. [22]. According to their conclusion, all the above three types of BCs are always applied to numerical examples in engineering practice. Since RS BC represents a symmetric analysis about the symmetric face, only half of the slope is required to perform the stability analysis for simplification. Therefore, the RS BC is selected for all the slope cases below.

2.5. Validation. For the purpose of validation of the numerical method used in this research, the typical slope example introduced by Zhang [23] is analyzed in this section. The geometry cross section of this slope is shown in Figure 3, which has a 10 m height and a gradient of $1V:2H$ (where V = vertical and H = horizontal). Material parameters of this slope are listed in Table 1. The extended width in the third dimension is 60 m. However, the actual mesh extended width in this paper is reduced by half of this amount because of the symmetry face.

Zhang [23] originally used an extended 3D Spencer's method to analyze this example. Since then, numerous investigators have used this model to validate their 3D slope stability methods (e.g., [12–14, 24–27]). To make as adequate of the comparisons with other results as possible, the same four cases, i.e., homogeneous soil slope (case 1), nonhomogeneous soil slope with a thin weak layer (case 2), homogeneous soil slope with a piezometric line (case 3), and nonhomogeneous soil slope with a piezometric line (case 4), are analyzed.

The FOS results for the four cases obtained by the present study and several other methods are given in Table 2. The FOS values obtained by the present study are 2.133, 1.512, 1.813, and 1.287 for cases 1, 2, 3, and 4, respectively, which demonstrate good consistency with the other solutions except for a slightly greater difference for case 2 (although still being 15%) between the results obtained by the modified SR-FEM and those of Chen et al. [26]. In contrast to the result of case 1, the FOS values of the other cases are remarkably decreased when a weak layer or groundwater existed within a slope, and the weak layer has a somewhat larger effect on the slope stability when compared to the groundwater effect. The FOS results of these analyses for the relatively simple validation example shown here indicate that results of the numerical FEM model lay well within the quite narrow range of results of the reference research for practical purposes.

3. Stability Charts for 3D Failures of Homogeneous Slopes

3.1. Stability Number for Homogeneous Soil Slopes. Sketch of the typical 3D slope model with a limited width W for the problem considered in this study is shown in Figure 4. To

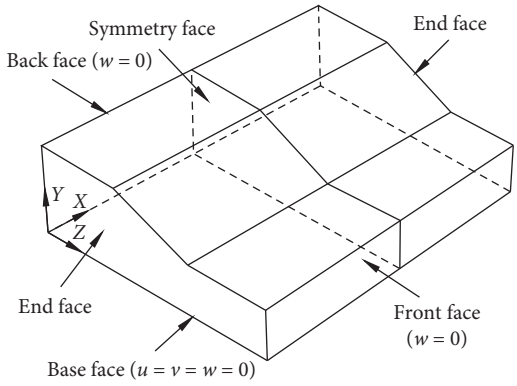

Figure 2: Typical 3D slope model and the BCs.

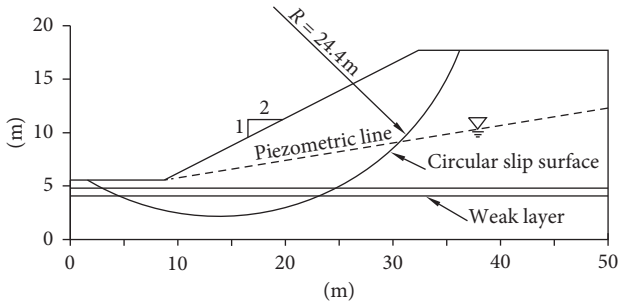

Figure 3: Cross section of the 3D slope reported by Zhang's [23] example.

Table 1: Material properties of Zhang's [23] example.

Material property	Upper soil layer	Weaker layer
Young's modulus, E (MPa)	10	10
Poisson's ratio, ν	0.25	0.25
Unit weight, γ (kN/m^3)	18.8	19.5
Friction angle, φ (°)	20	10
Cohesion, c (kPa)	29	0
Dilation angle, ψ (°)	0	0

Table 2: Comparison of the FOS of the four slope cases based on various methods.

Case	Source	FOS
1	2D (average) by Fredlund and Krahn [24]	2.034
	3D-LEM CLARA by Hungr [25]	2.167
	3D LEM by Zhang [23]	2.122
	3D UB-LAM by Chen et al. [26]	2.262
	3D-LEM by Chen et al. [27]	2.187
	3D-FEM by Griffiths and Marquez [12]	2.17
	3D-FEM by Nian et al. [13]	2.15
	3D-FDM by Zhang et al. [14]	2.18
	Present solution	2.133
2	2D (average) by Fredlund and Krahn [24]	1.383
	3D-LEM CLARA by Hungr [25]	1.62
	3D LEM by Zhang [23]	1.553
	3D UB-LAM by Chen et al. [26]	1.717
	3D-LEM by Chen et al. [27]	1.603
	3D-FEM by Griffiths and Marquez [12]	1.58
	3D-FEM ABAQUS by Nian et al. [13]	1.52
	Present solution	1.512
3	2D (average) by Fredlund and Krahn [24]	1.799
	3D-FEM ABAQUS by Nian et al. [13]	1.86
	Present solution	1.813
4	2D (average) by Fredlund and Krahn [24]	1.441
	3D-FEM ABAQUS by Nian et al. [13]	1.298
	Present solution	1.287

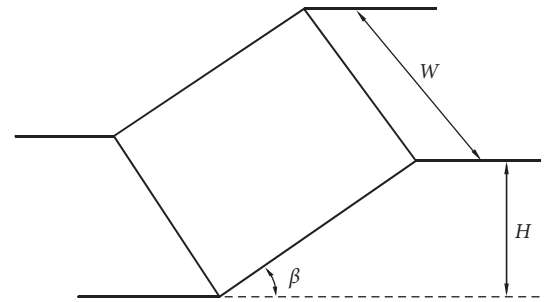

Figure 4: Sketch of the typical 3D slope model with a limited width W.

study the 3D effect on stability analysis, the 3D slope model in this paper is obtained by extending the 2D slope profile (x-y plane) in the width direction (z direction) by a distance of W (W = length into the page of the slope profile). For the purpose of reducing the mesh size and saving the computation time, this extension is done symmetrically. In present paper, a series of slope angles $\beta = 15^\circ, 30^\circ, 45^\circ, 60^\circ, 75^\circ$, and 90° are studied and various magnitudes of ratios of W/H ranging from 0.5, 0.6, 0.8, 1.0, 2.0, 3.0, 5.0, and 10 are investigated. In general, as illustrated in Figure 1, failure modes of the soil slope falls into three types, namely, face failure, toe failure, and base failure.

One problem in developing stability charts for determining the FOS is that numerous parameters are included (Figure 4), such as the slope angle (β), the slope height (H), the slope width W, the unit weight of the soil (γ), the cohesion strength c and internal fictional angle φ, and the horizontal seismic acceleration coefficient k_h. Based on previous research results, the number of variables in stability analysis can be reduced through appropriate use of dimensionless parameters that make the stability charts more concise. In general, there are five significant dimensionless parameters in developing the slope stability charts. A dimensionless parameter $\lambda_{c\varphi}$ is used in this paper, which was proposed by Bell [28] as follows:

$$\lambda_{c\varphi} = \frac{c_f}{\gamma H \tan \varphi_f} = \frac{c/F}{\gamma H \tan \varphi / F} = \frac{c}{\gamma H \tan \varphi}, \tag{5}$$

in which F is the FOS. $F/\tan\varphi$ is defined as the stability number of a slope and is a function of the dimensionless parameter $\lambda_{c\varphi}$. The FOS will be calculated with no iteration. In addition, FOS for undrained purely cohesive soil slopes ($\varphi = 0$) may be calculated with no iteration according to the stability number $c_d/\gamma H = c_u/\gamma HF$, where c_u is the undrained cohesion.

3.2. Stability Charts for 3D Failures of Purely Cohesive Soil Slopes. For 3D homogeneous purely cohesive soil slopes ($\varphi = 0$), the relationship between the critical values of stability number $c_u/\gamma HF$ against the slope angles is shown in Figure 5 for slopes with a series of ratios of W/H under the condition of static ($k_h = 0$) and pseudostatic seismic loading ($k_h = 0.1$, 0.2, and 0.3). It can be noticed that the critical values of $c_u/\gamma HF$ are inclined to infinity when the 3D homogeneous slopes in purely cohesive soils with the gentle inclination angle suffer from stronger seismic excitation. A method by constraining the depth of the slip surface to an actual value D below slope crest (Figure 1) is adopted to reduce the computing scale and obtain a more rational value. According to the results, the depth factor (D/H) has little effect on the FOS of slopes when $D/H \geq 2.0$. Thus, $D/H = 2.0$ is available for determination of the 3D mechanism for the slopes under the effect of seismic excitation. Furthermore, it can be seen that, as expected, the FOS of homogeneous purely cohesive soil slopes decreases with an increase in values of slope angle β, horizontal acceleration k_h, and ratio W/H.

Additionally, the charts in Figure 5 also show the corresponding type of slope failure modes, i.e., solid curves representing the toe-failure mode, dashed curves representing the face-failure mode, and dotted curves representing the base-failure mode. It is also significant to note that the type of the critical failure mode varies from base failure to toe failure for 3D slopes owing large ratios of $W/H \geq 1.0$ when the slope angle β reaches a certain threshold value. However, the critical values of $c_u/\gamma HF$ are determined as well as the face-failure mechanism for 3D homogeneous slopes with small ratios of W/H.

3.3. Stability Charts for 3D Failures of Cohesive-Frictional Soil Slopes. In the case of 3D homogeneous cohesive-frictional soil slopes ($\varphi > 0$), stability charts for the 2D case and for various cases with W/H ratios ranging from 0.5 to 10 under the conditions of static and seismic loading are illustrated in Figures 6–9. As can be seen from Figures 6–9, $F/\tan\varphi$ increases with the increasing dimensionless parameter $c/\gamma H \tan\varphi$, decreasing ratio W/H, the magnitude of the horizontal acceleration coefficient k_h, and slope angle β. Compared to Figure 4, the charts in Figures 5–7 show that applying the quasistatic horizontal force significantly reduces the FOS of the slopes. The decrease is more remarkable for gentler slopes with large values of ratios W/H under the stronger seismic excitation effect as indicated by having diverging W/H trend lines for slopes with high k_h values at small values of β. Such decrease in the sensitivity of the FOS to changes in k_h, which reflects the influences of quasistatic forces in gravitational or vertical direction based on its definition, can be considered in relation to the increasing impact of the equivalent horizontal static forces on slope safety under the condition of high seismicity. Vertical distance between these chart lines represents the FOS differences for 3D and 2D slopes, respectively. Each chart in Figures 6–9 represents the FOS for one slope angle. By means of referring to these charts, the type of failure modes can also be obtained as well.

It may be obviously noticed that the toe-failure mode yields the critical values of $c/\gamma H \tan\varphi$ for the most part. When the 3D slope width is limited to a small value, the toe-failure mode cannot be developed as a result of the geometric constraints. However, with regard to small ratios of W/H ($W/H \leq 1.0$), the face-failure mode is developed within the slope and yields the critical values of $c/\gamma H \tan\varphi$. Slopes with a gentle angle have a great tendency to construct the base-failure mode. Nevertheless, the base-failure mode can also be found in some steeper cases under the effect of stronger seismic excitation.

3.4. Example of Application. The following hypothetical example illustrates applications of the previously presented stability charts (Figures 5–9) in this paper, as well as the significance of considering the seismic excitation effect on the stability analysis of homogeneous slopes. From these charts, FOS, as well as the type of failure modes, is easily determined for 3D failures of cohesive-frictional soil and purely cohesive soil slopes under the conditions of static and pseudostatic seismic effects. The example is described as follows.

A 3D homogeneous slope with a height of 10 m and an inclination angle of 30° under the pseudostatic seismic loading condition (the value of the horizontal acceleration coefficient $k_h = 0.3$) is utilized to exhibit the application of presented stability charts. Material parameters for the soil are $\gamma = 18\ \text{kN/m}^3$, $\varphi = 15°$, and $c = 40\ \text{kPa}$. Width of the slope is constrained by rock formations and spreads 20 m apart ($W/H = 2.0$). Hence, $c/\gamma H \tan\varphi = 40/18 \times 10 \times \tan 15° = 0.83$. For $\beta = 30°$ and $k_h = 0.3$, it can be determined from Figure 9 that $F/\tan\varphi = 6.14$. Based on the above equation, the factor of safety F was calculated to be 1.64, and the slope failure mode is found to be base failure from Figure 9. However, the FOS of this slope with no consideration of the seismic excitation effect could be obtained from Figure 6 as $F = 2.85$, and the corresponding type of the slope failure mode is toe failure.

4. Comparison with Other Charts

In this section, the proposed chart solutions for 3D homogeneous slopes are compared with results obtained by other methods under static conditions to further validate the strength reduction analysis in this research. Figure 10 gives the comparisons between the critical values of $c_u/\gamma HF$ obtained from this paper and those from the limit equilibrium method by Gens et al. [6] and the rigorous analytical limit analysis method by Gao et al. [10] for slopes in purely cohesive soils with various ratios of W/H. As can be obviously seen in Figure 10, the trends exhibited by the strength reduction results are in good agreement with those of Gens et al. [6] and Gao et al. [10].

Recently, Li et al. [8] used the numerical limit analysis method to propose stability charts for 3D homogeneous slopes in frictional/cohesive soils. As illustrated in Figure 11, comparisons are carried out between the chart solutions from this paper and the numerical upper- and

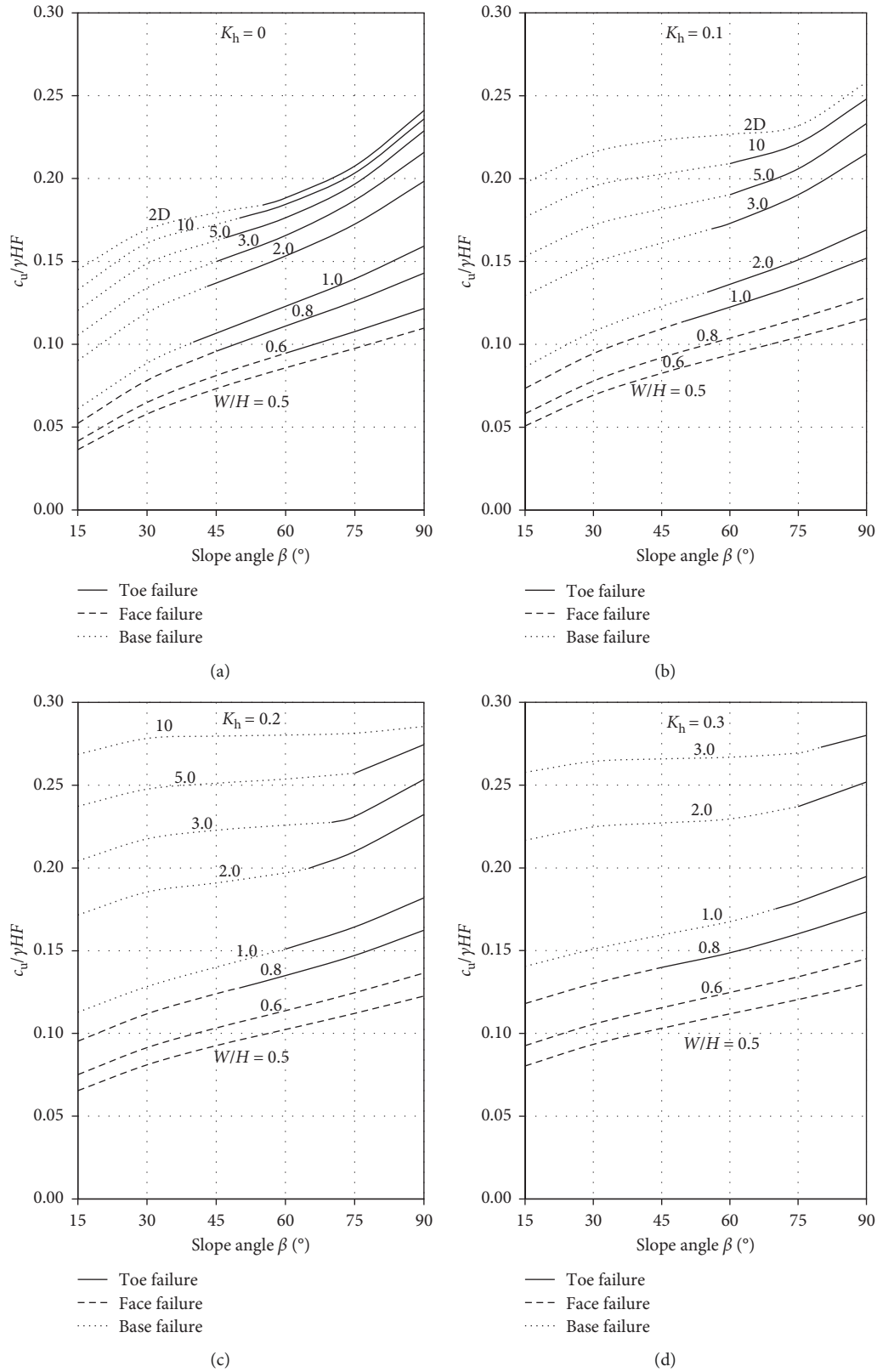

Figure 5: Stability charts for 3D failures of purely cohesive soil slopes under static and pseudostatic seismic conditions.

lower-bound solutions obtained from Li et al. [8] for various slope angles. It can be noted that the SRM solutions of this study are closely bracketed by the numerical upper- and lower-bound solutions. It shows good consistency with the findings of chart solutions by Sun et al. [22]. Therefore, the failure mechanisms adopted in this

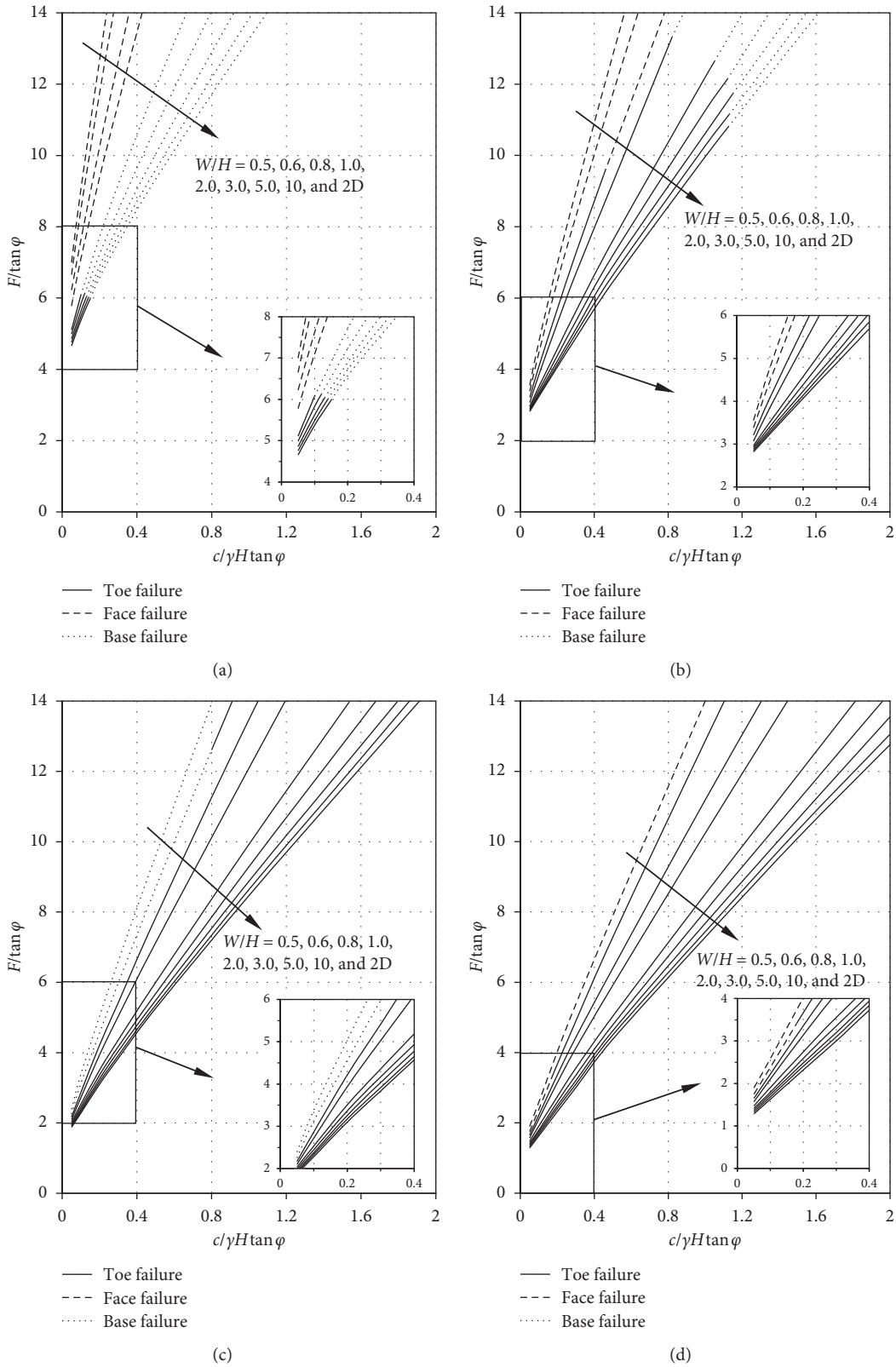

Figure 6: Continued.

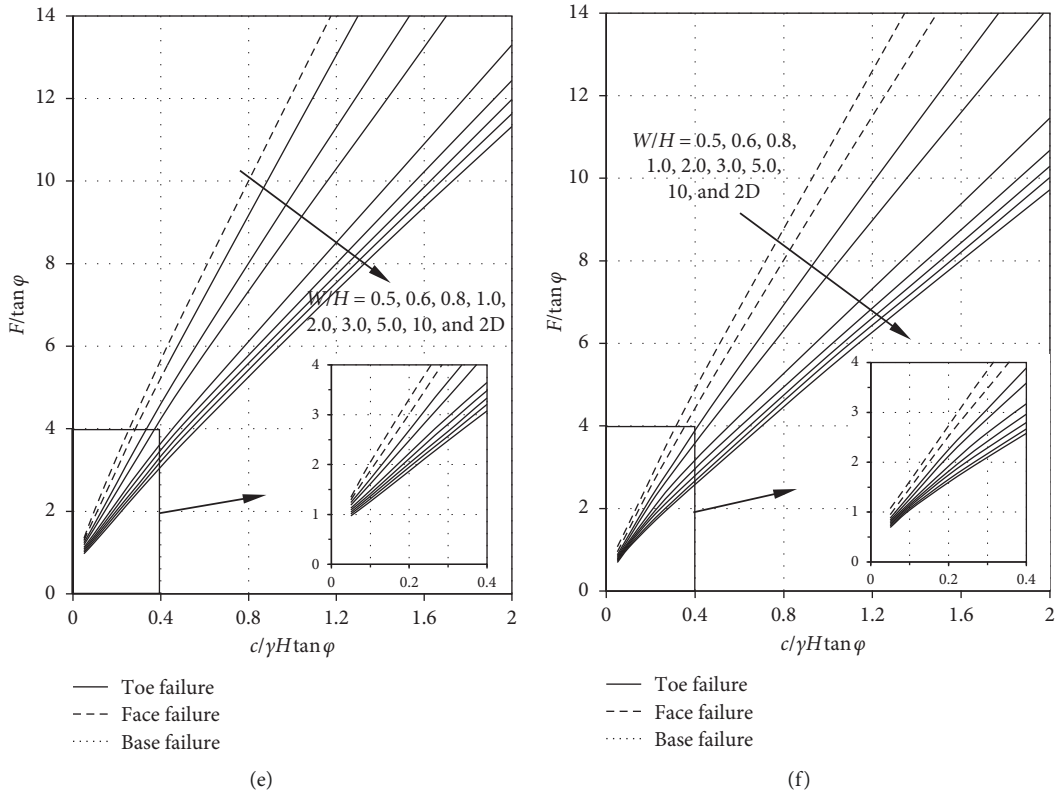

Figure 6: Stability charts for 3D failures of cohesive-frictional soil slopes under static conditions: (a) $\beta = 15^{\circ}$; (b) $\beta = 30^{\circ}$; (c) $\beta = 45^{\circ}$; (d) $\beta = 60^{\circ}$; (e) $\beta = 75^{\circ}$; (f) $\beta = 90^{\circ}$.

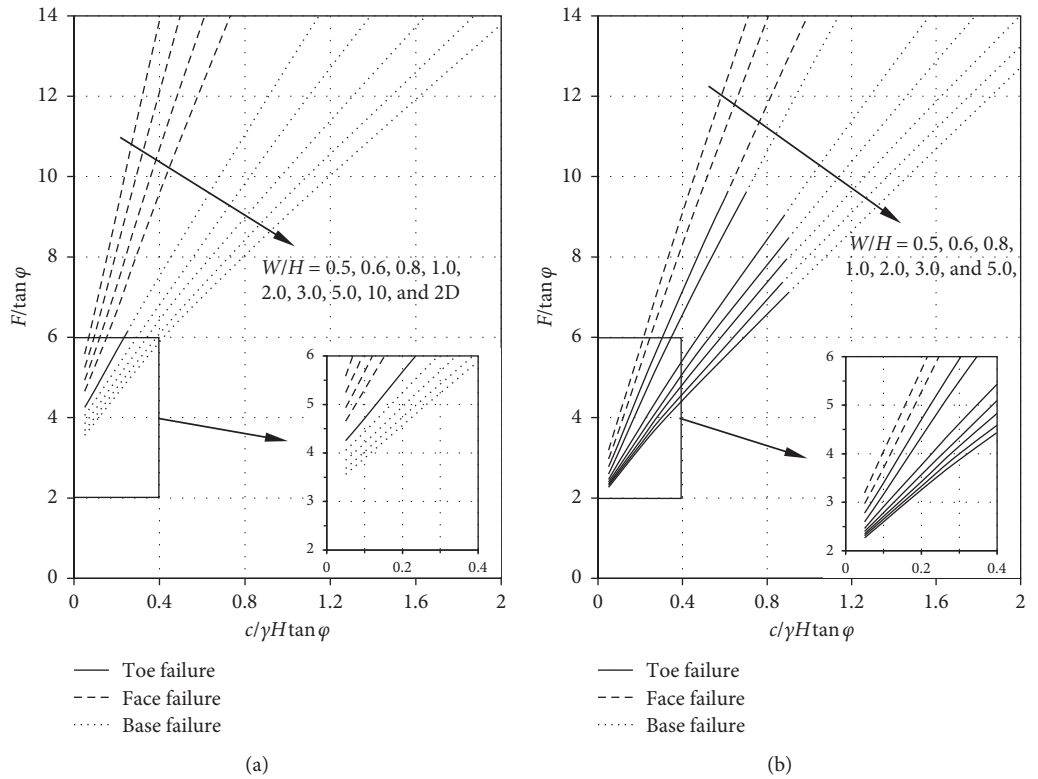

Figure 7: Continued.

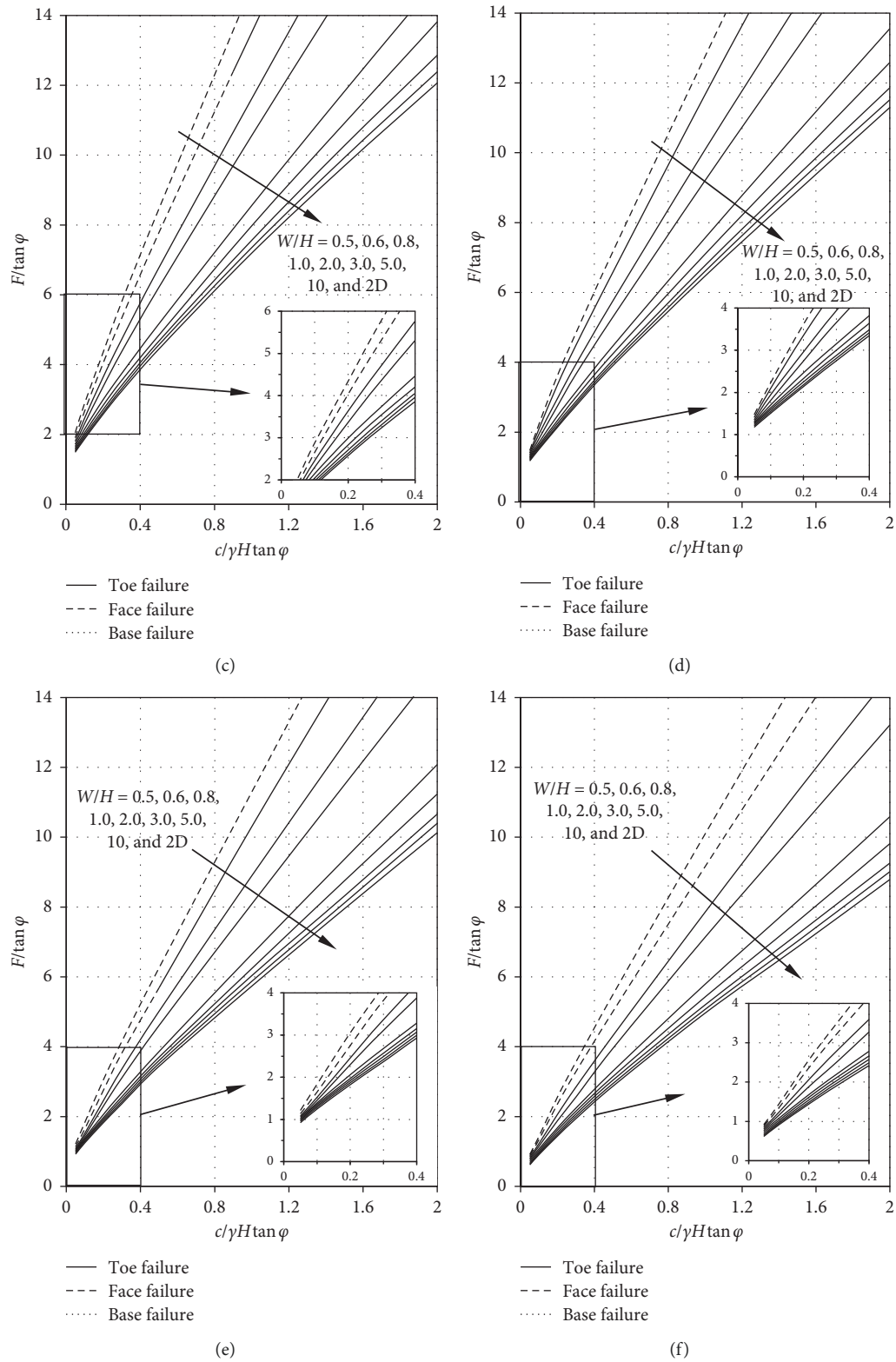

Figure 7: Stability charts for 3D failures of cohesive-frictional soil slopes under seismic conditions with $k_h = 0.1$: (a) $\beta = 15^\circ$; (b) $\beta = 30^\circ$; (c) $\beta = 45^\circ$; (d) $\beta = 60^\circ$; (e) $\beta = 75^\circ$; (f) $\beta = 90^\circ$.

study can provide a good way to estimate the stability of 3D homogeneous slopes in both purely cohesive and frictional/cohesive soils.

To further investigate the difference in the FOS between this study and the numerical limit analysis, the example adopted by Li et al. [8] is used here. The slope is described as

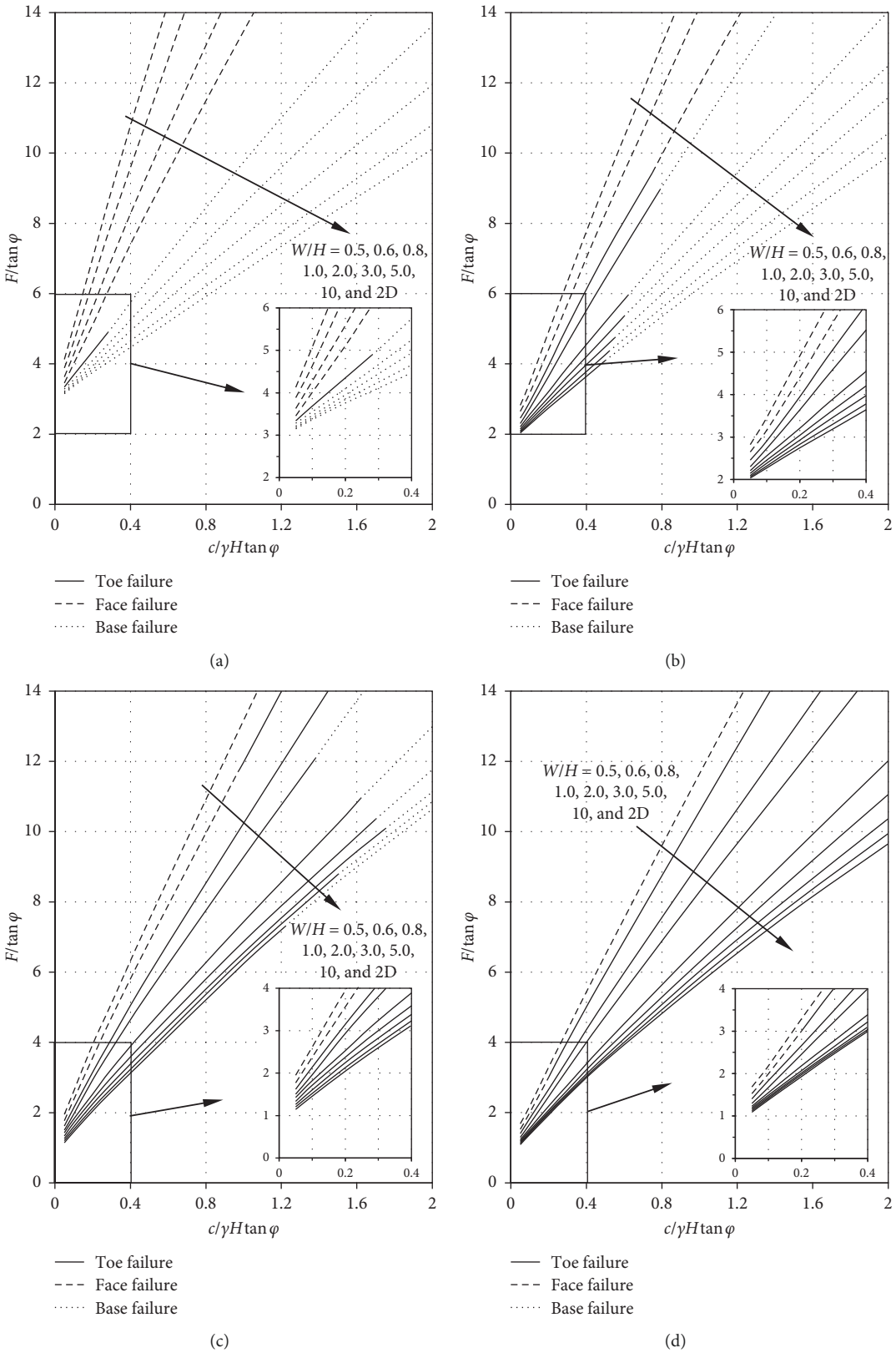

Figure 8: Continued.

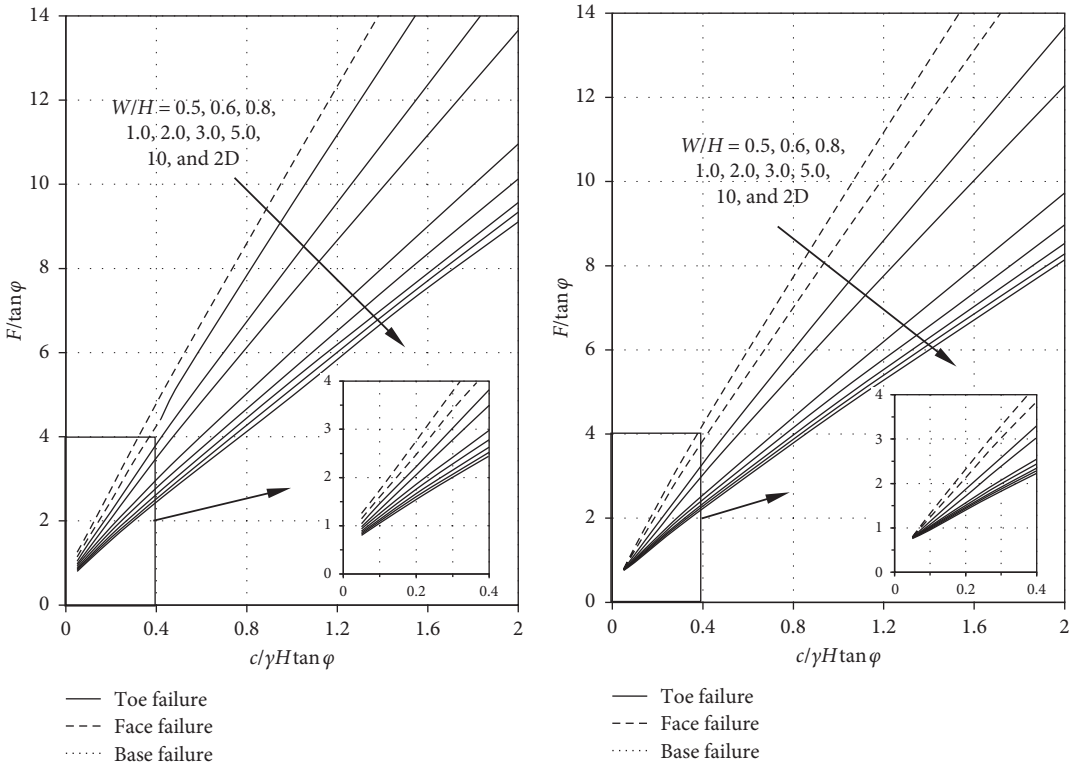

Figure 8: Stability charts for 3D failures of cohesive-frictional soil slopes under seismic conditions with $k_h = 0.2$: (a) $\beta = 15^\circ$; (b) $\beta = 30^\circ$; (c) $\beta = 45^\circ$; (d) $\beta = 60^\circ$; (e) $\beta = 75^\circ$; (f) $\beta = 90^\circ$.

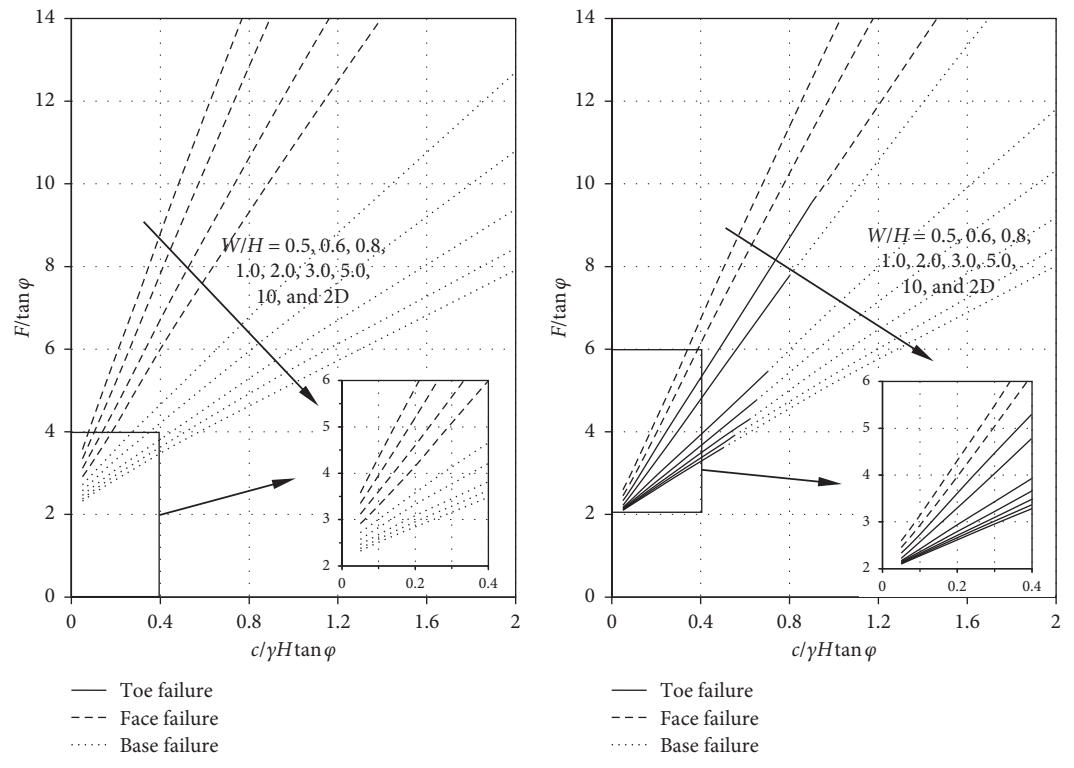

Figure 9: Continued.

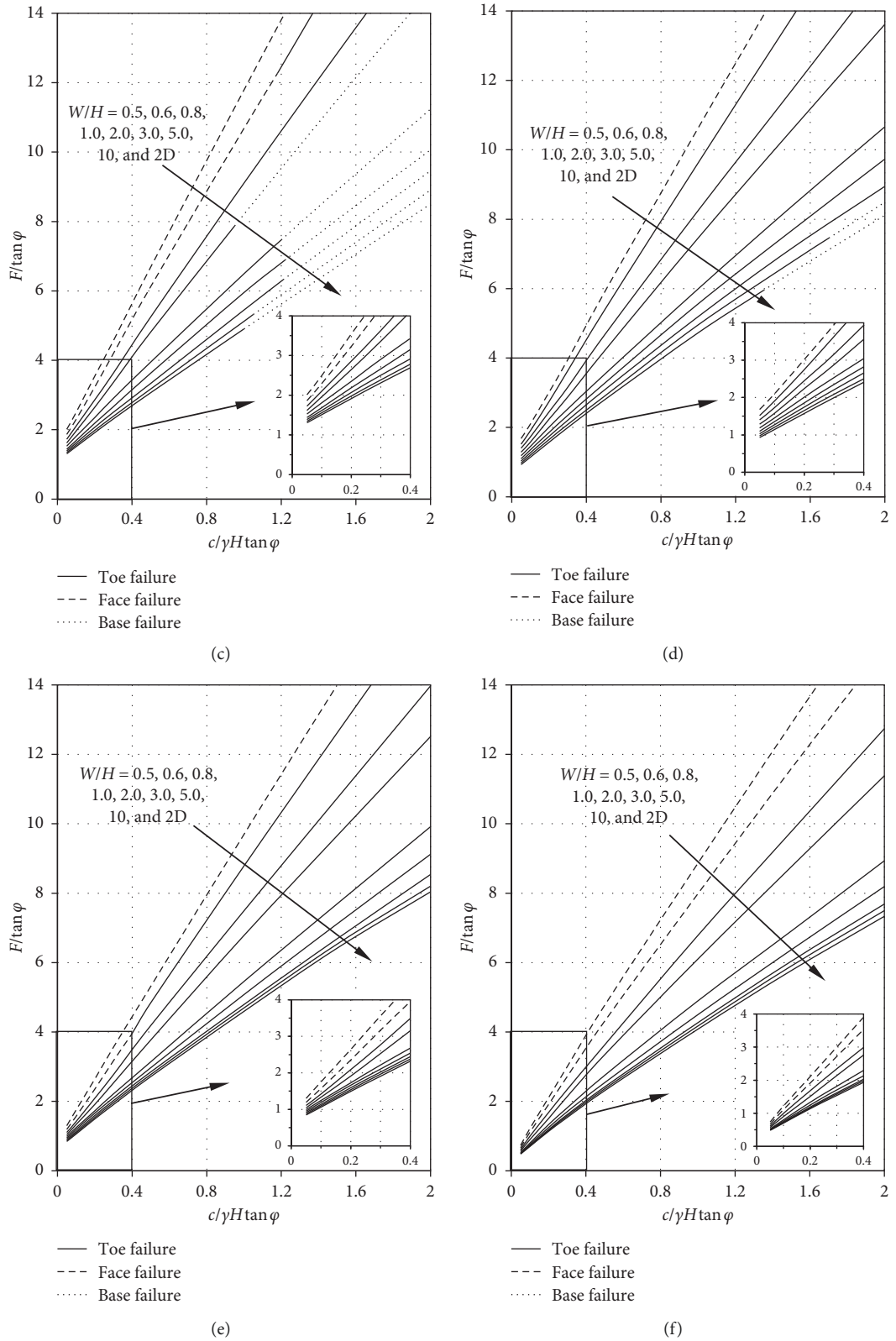

Figure 9: Stability charts for 3D failures of cohesive-frictional soil slopes under seismic conditions with $k_h = 0.3$: (a) $\beta = 15^\circ$; (b) $\beta = 30^\circ$; (c) $\beta = 45^\circ$; (d) $\beta = 60^\circ$; (e) $\beta = 75^\circ$; (f) $\beta = 90^\circ$.

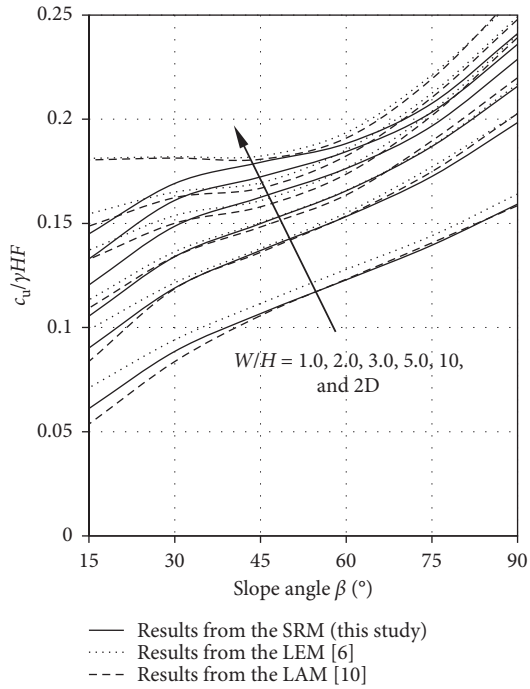

Figure 10: Comparisons between the critical values of $c_u/\gamma HF$ obtained from this paper and those from Gens et al. [6] and Gao et al. [10] for undrained slopes.

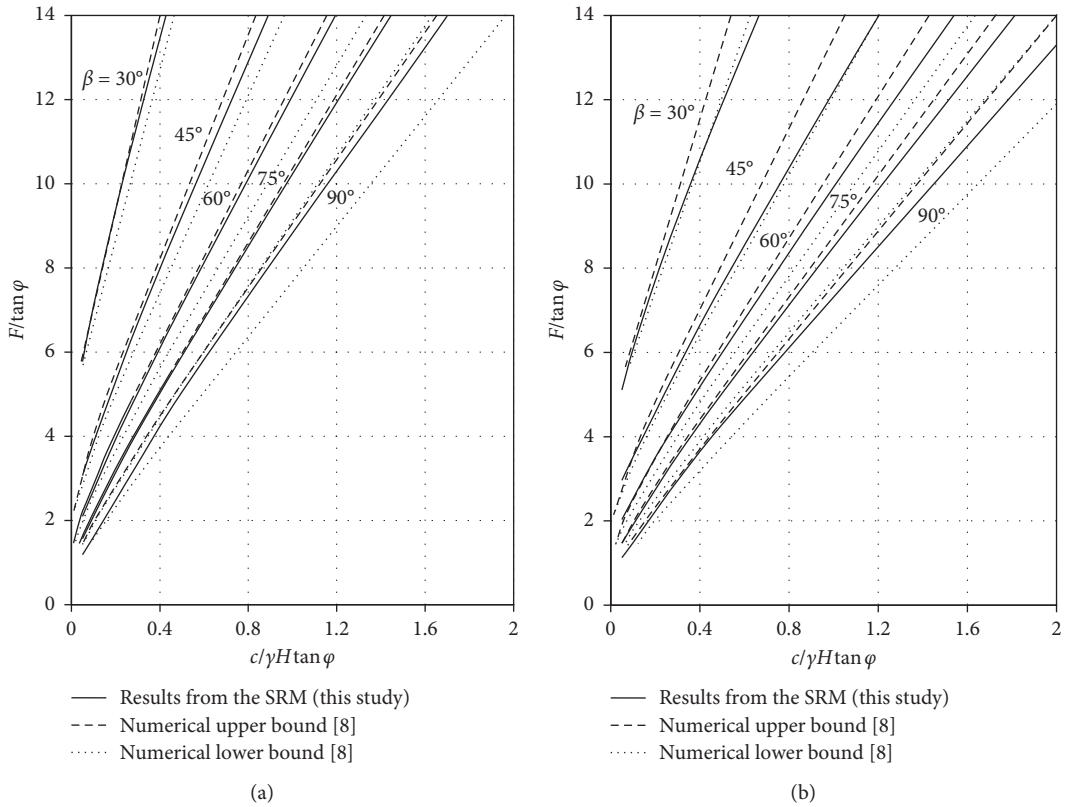

Figure 11: Continued.

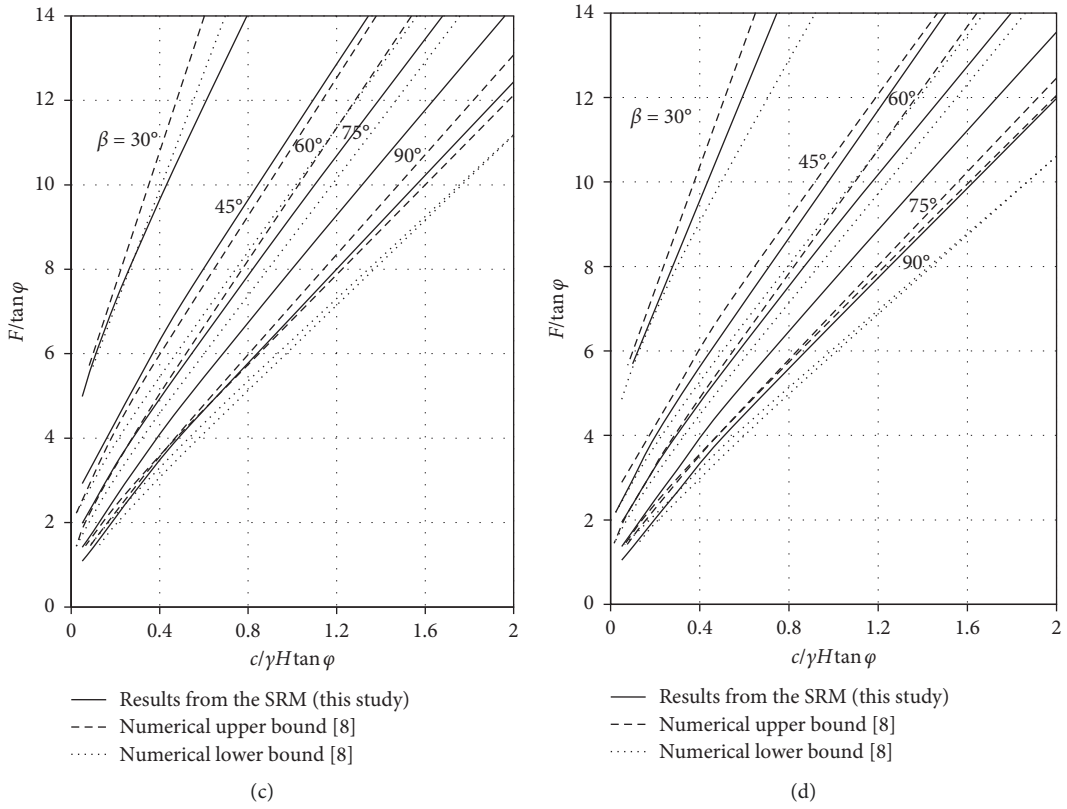

Figure 11: Comparisons between the chart solutions of this study and the upper- and lower-bound solutions from Li et al. [8] for 3D frictional/cohesive soil slopes with various W/H ratios: (a) $W/H = 1.0$; (b) $W/H = 2.0$; (c) $W/H = 3.0$; (d) $W/H = 5.0$.

Table 3: Comparisons between calculated results of the FOS derived from this study and the upper- and lower-bound solutions presented by Li et al. [8] for the example slope.

Method	Safety factor	$W/H = 1.0$	$W/H = 2.0$	$W/H = 3.0$	$W/H = 5.0$	$W/H = 10$	2D
Chart solution (present study)	$F/\tan\varphi$	5.31	4.54	4.31	4.14	4.03	3.75
	F	1.42	1.22	1.15	1.11	1.08	1.00
Numerical upper bound [8]	$F/\tan\varphi$	5.35	4.55	4.25	4.20	—	3.80
	F	1.44	1.22	1.14	1.13	—	1.02
Numerical lower bound [8]	$F/\tan\varphi$	4.75	4.05	3.95	3.80	—	3.70
	F	1.27	1.09	1.06	1.02	—	0.99

frictional angle $\varphi = 15^\circ$, slope angle $\beta = 60^\circ$, and stability number $c/\gamma H\tan\varphi \approx 0.433$. Table 3 shows the calculated results of the FOS obtained from the presented charts in this paper and those from the numerical limit analyses. It can be concluded that almost all the present results in Table 3 based on SRM are obviously closed to those from the numerical limit analysis method, falling between the numerical lower bound and the numerical upper bound for all cases examined, except for the case of $W/H = 3.0$.

5. Discussion

Based on all numerical results of the several hundred cases that have been considered, it is observed that the FOS and the corresponding failure modes with different geometries, the horizontal acceleration coefficients, slope angle, and material properties are different. In fact, the effects of any geometry on 3D slope stability are reflected by two aspects: change in area of the sliding surface and change in volume of the failure mass, which are relative to common 3D slope under the same boundary condition. The variation in FOS depends on these changes. Figures 12–15 show contours of the maximum shear strain increment with factors of safety for various 3D slope cases obtained from this study. These contours can be seen as the failure mechanism [29].

Figure 12 shows that the failure mechanisms are closer to a toe-failure mode when the W/H ratio is less than 1.0. With the increase in slope width W ($W/H \geq 2.0$), the depth of the critical slip surface becomes deeper, which belongs to the base-failure modes. Additionally, it is interesting to find that slip surfaces on symmetry face remain little changed with different widths of the slip surface. This effect explains the

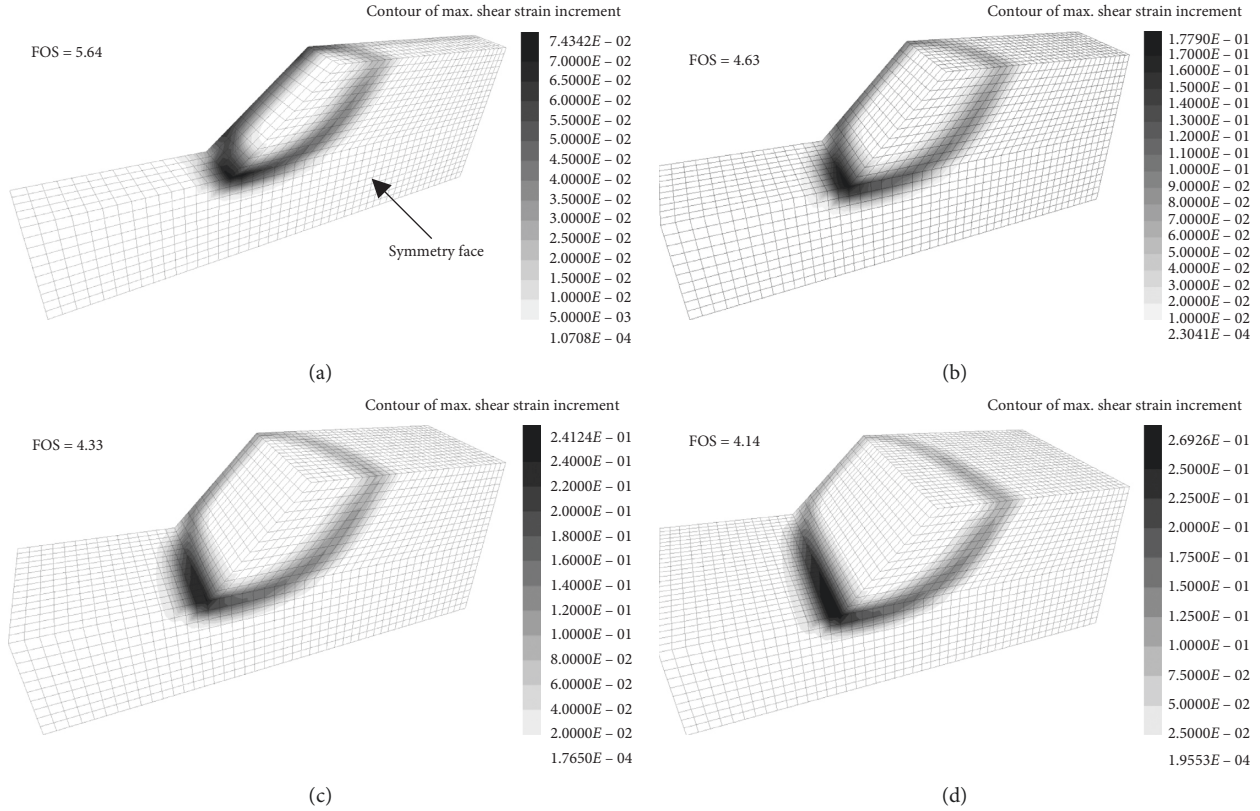

Figure 12: Contours of the maximum shear strain increment with factors of safety for 3D slopes with various W/H ratios when $\beta = 45^{\circ}$, $K_h = 0$, and $\lambda_{c\varphi} = 1.0$: (a) $W/H = 1.0$; (b) $W/H = 2.0$; (c) $W/H = 3.0$; (d) $W/H = 5.0$.

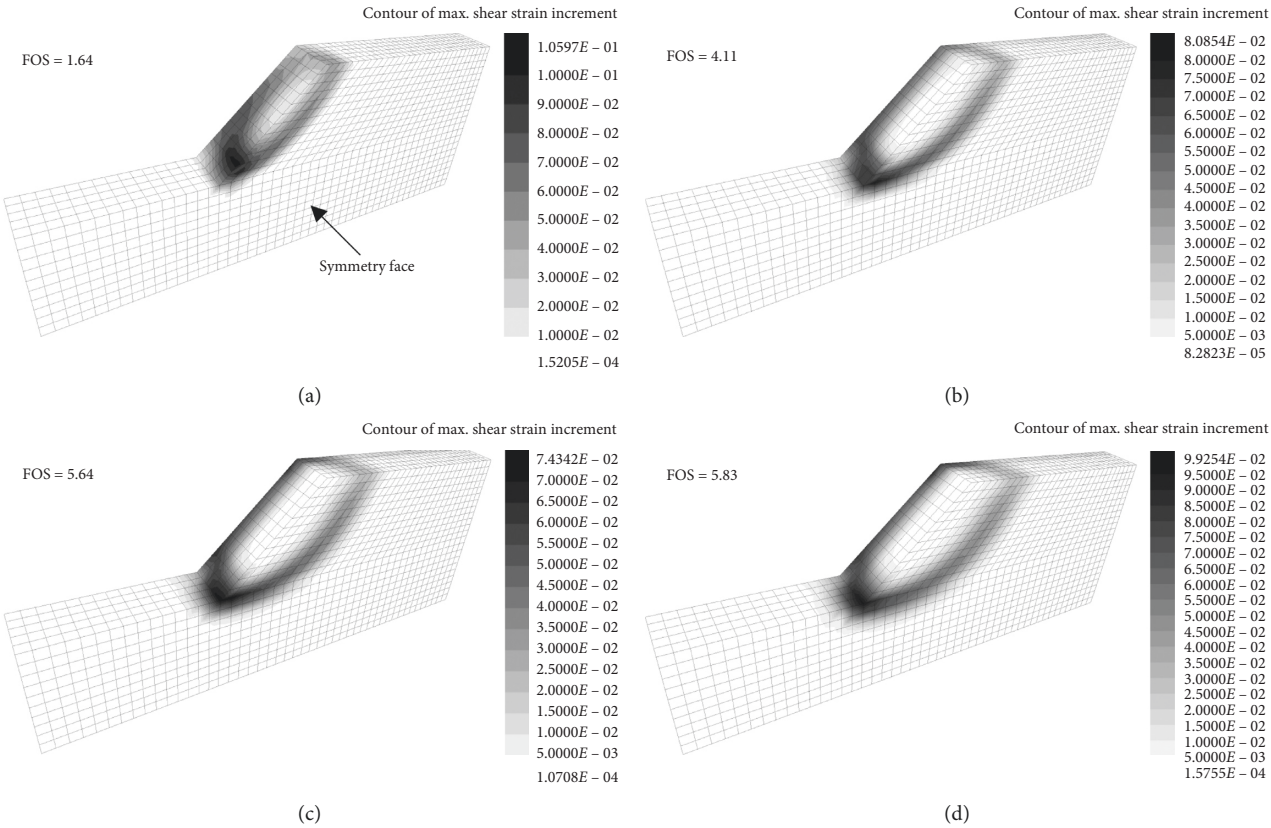

Figure 13: Contours of the maximum shear strain increment with factors of safety for 3D slopes with various $\lambda_{c\varphi}$ values when $\beta = 45^{\circ}$, $W/H = 1.0$, and $K_h = 0$: (a) $\lambda_{c\varphi} = 0.05$; (b) $\lambda_{c\varphi} = 0.5$; (c) $\lambda_{c\varphi} = 1.0$; (d) $\lambda_{c\varphi} = 2.0$.

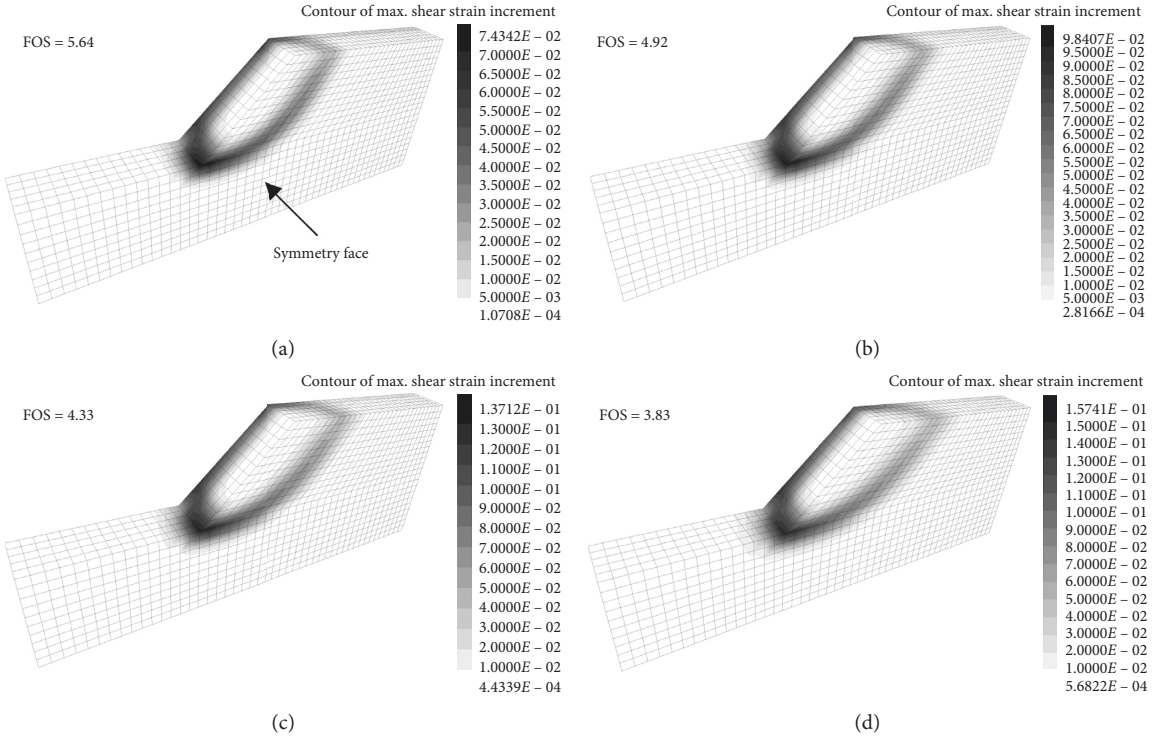

Figure 14: Contours of the maximum shear strain increment with factors of safety for 3D slopes with various K_h values when $\beta = 45^\circ$, $W/H = 1.0$, and $\lambda_{c\varphi} = 1.0$: (a) $K_h = 0$; (b) $K_h = 0.1$; (c) $K_h = 0.2$; (d) $K_h = 0.3$.

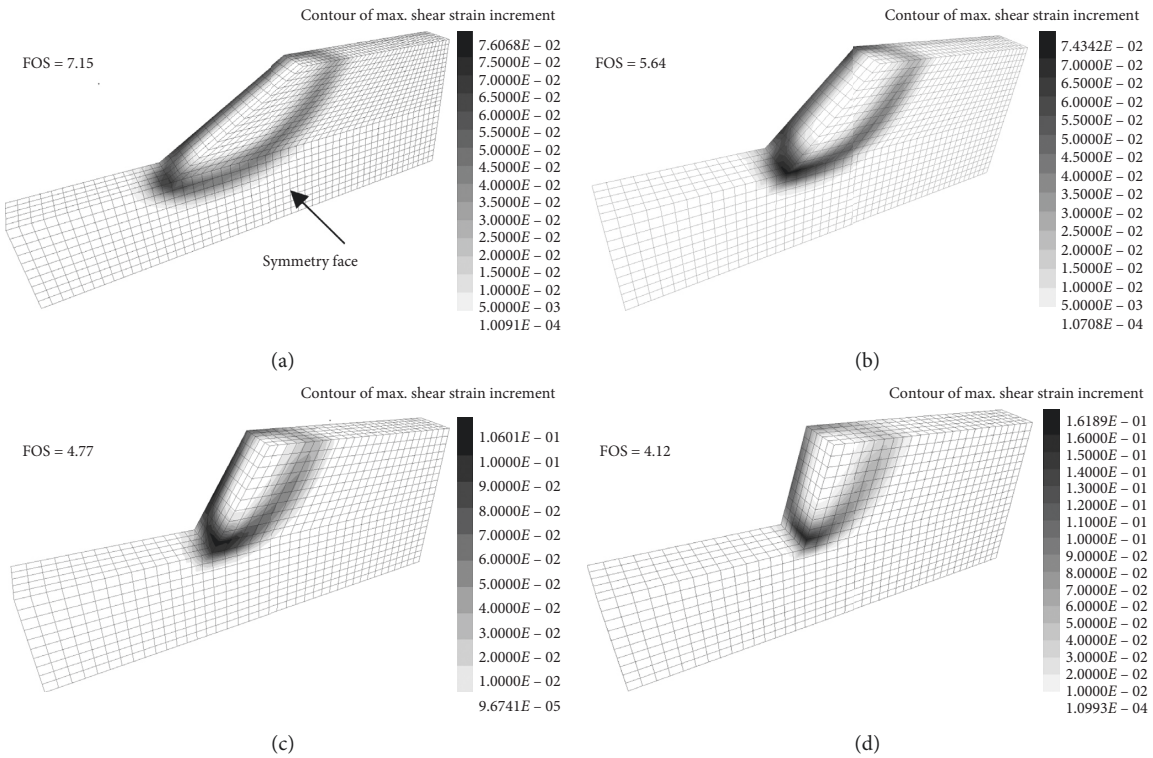

Figure 15: Contours of the maximum shear strain increment with factors of safety for 3D slopes with various β values when $K_h = 0$, $W/H = 1.0$, and $\lambda_{c\varphi} = 1.0$: (a) $\beta = 30^\circ$; (b) $\beta = 45^\circ$; (c) $\beta = 60^\circ$; (d) $\beta = 75^\circ$.

results where the FOS decreases slightly when W/H ratio increases. From Figures 13 and 14, it can be observed that the dimensionless parameter $\lambda_{c\varphi}$ and the horizontal acceleration coefficient K_h have a significant effect on both the FOS and failure modes. The FOS increases remarkably when $\lambda_{c\varphi}$ increases from 0.05 to 2.0 and K_h decreases from 0.3 to 0. The failure mechanism varies from the face-failure mode to the base-failure mode with the increase of $\lambda_{c\varphi}$ and K_h. As for Figure 15, when the slope angle becomes steeper, the FOS decreases dramatically and the depth of the critical slip surface decreases obviously, which means the failure modes change from base failure to face failure.

6. Conclusions

On the basis of the 3D rotational slope failure mode, this paper produces stability charts for pseudostatic stability analysis of 3D homogeneous soil slopes under the horizontal seismic condition. The presented charts can be used in preliminary design of slope engineering, and allow the designers to estimate the FOS of the slope without the need of any iterative process and identify the corresponding type of the critical slope failure mode. Further work will consider the effects of other typical factors such as pore water pressure and surcharge load on slope stability analysis.

Data Availability

The data used to support the findings of this study are available from the corresponding author upon request.

Conflicts of Interest

The authors declare that they have no conflicts of interest.

Acknowledgments

This research was financially supported by the National Natural Science Foundation of China (51679197), the Natural Science Foundation Research Project of Shaanxi Province (2017JZ013), the Scientific Research Staring Foundation for Introduced Talents of Xijing University (XJ18T05), and the Science and Technology Project of Guizhou Province (20161154). All the financial supports are greatly appreciated.

References

[1] D. W. Taylor, "Stability of earth slopes," *Journal of the Boston Society of Civil Engineers*, vol. 24, no. 3, pp. 197–246, 1937.

[2] R. L. Michalowski, "Stability charts for uniform slopes," *Journal of Geotechnical and Geoenvironmental Engineering*, vol. 128, no. 4, pp. 351–355, 2002.

[3] R. Baker, "A second look at Taylor's stability chart," *Journal of Geotechnical and Geoenvironmental Engineering*, vol. 129, no. 12, pp. 1102–1108, 2003.

[4] T. Steward, N. Sivakugan, S. K. Shukla, and B. M. Das, "Taylor's slope stability charts revisited," *International Journal of Geomechanics*, vol. 11, no. 4, pp. 348–352, 2011.

[5] R. L. Michalowski, "Limit analysis and stability charts for 3D slope failures," *Journal of Geotechnical and Geoenvironmental Engineering*, vol. 136, no. 4, pp. 583–593, 2010.

[6] A. Gens, J. N. Hutchinson, and S. Cavounidis, "Three-dimensional analysis of slides in cohesive soils," *Géotechnique*, vol. 38, no. 1, pp. 1–23, 1988.

[7] A. J. Li, R. S. Merifield, and A. V. Lyamin, "Limit analysis solutions for three dimensional undrained slopes," *Computers and Geotechnics*, vol. 36, no. 8, pp. 1330–1351, 2009.

[8] A. J. Li, R. S. Merifield, and A. V. Lyamin, "Three-dimensional stability charts for slopes based on limit analysis methods," *Canadian Geotechnical Journal*, vol. 47, no. 12, pp. 1316–1334, 2010.

[9] R. L. Michalowski and T. Martel, "Stability charts for 3D failures of steep slopes subjected to seismic excitation," *Journal of Geotechnical and Geoenvironmental Engineering*, vol. 137, no. 2, pp. 183–189, 2011.

[10] Y. Gao, F. Zhang, G. H. Lei, D. Li, Y. Wu, and N. Zhang, "Stability charts for 3D failures of homogeneous slopes," *Journal of Geotechnical and Geoenvironmental Engineering*, vol. 139, no. 9, pp. 1528–1538, 2013.

[11] H. Zheng, D. F. Liu, and C. G. Li, "Slope stability analysis based on elasto-plastic finite element method," *International Journal for Numerical Methods in Engineering*, vol. 64, no. 14, pp. 1871–1888, 2005.

[12] D. V. Griffiths and R. M. Marquez, "Three-dimensional slope stability analysis by elasto-plastic finite elements," *Géotechnique*, vol. 57, no. 6, pp. 537–546, 2007.

[13] T.-K. Nian, R.-Q. Huang, S.-S. Wan, and G.-Q. Chen, "Three-dimensional strength-reduction finite element analysis of slopes: geometric effects," *Canadian Geotechnical Journal*, vol. 49, no. 5, pp. 574–588, 2012.

[14] Y. Zhang, G. Chen, L. Zheng, Y. Li, and X. Zhuang, "Effects of geometries on three-dimensional slope stability," *Canadian Geotechnical Journal*, vol. 50, no. 3, pp. 233–249, 2013.

[15] C. Sun, J. Chai, Z. Xu, Y. Qin, and X. Chen, "Stability charts for rock mass slopes based on the Hoek-Brown strength reduction technique," *Engineering Geology*, vol. 214, pp. 94–106, 2016.

[16] R. Baker, R. Shukha, V. Operstein, and S. Frydman, "Stability charts for pseudostatic slope stability analysis," *Soil Dynamics and Earthquake Engineering*, vol. 26, no. 9, pp. 813–823, 2006.

[17] P. A. Lane and D. V. Griffiths, "Slope stability analysis by finite elements," *Géotechnique*, vol. 49, no. 3, pp. 387–403, 1999.

[18] Q. Xu, H. Yin, X. Cao, and Z. Li, "A temperature-driven strength reduction method for slope stability analysis," *Mechanics Research Communications*, vol. 36, no. 2, pp. 224–231, 2009.

[19] E. M. Dawson, W. H. Roth, and A. Drescher, "Slope stability analysis by strength reduction," *Géotechnique*, vol. 49, no. 6, pp. 835–840, 1999.

[20] T. Matsui and K.-C. San, "Finite element slope stability analysis by shear strength reduction technique," *Soils and Foundations*, vol. 32, no. 1, pp. 59–70, 1992.

[21] H. Zheng, D. F. Liu, and C. G. Li, "On the assessment of failure in slope stability analysis by the finite element method," *Rock Mechanics and Rock Engineering*, vol. 41, no. 4, pp. 629–639, 2008.

[22] C. W. Sun, J. R. Chai, Z. G. Xu, and Y. Qin, "3D stability charts for convex and concave slopes in plan view with homogeneous soil based on the strength-reduction method," *International Journal of Geomechanics*, vol. 17, no. 5, article 06016034, 2017.

[23] X. Zhang, "Three-dimensional stability analysis of concave slopes in plan view," *Journal of Geotechnical Engineering*, vol. 114, no. 6, pp. 658–671, 1988.

[24] D. G. Fredlund and J. Krahn, "Comparison of slope stability methods of analysis," *Canadian Geotechnical Journal*, vol. 14, no. 3, pp. 429–439, 1977.

[25] O. Hungr, "An extension of Bishop's simplified method of slope stability analysis to three dimensions," *Géotechnique*, vol. 37, no. 1, pp. 113–117, 1987.

[26] Z. Chen, X. Wang, C. Haberfield, J.-H. Yin, and Y. Wang, "A three-dimensional slope stability analysis method using the upper bound theorem," *International Journal of Rock Mechanics and Mining Sciences*, vol. 38, no. 3, pp. 369–378, 2001.

[27] J. Chen, J.-H. Yin, and C. F. Lee, "Upper bound limit analysis of slope stability using rigid finite elements and nonlinear programming," *Canadian Geotechnical Journal*, vol. 40, no. 4, pp. 742–752, 2003.

[28] J. M. Bell, "Dimensionless parameters for homogeneous earth slopes," *Journal of the Soil Mechanics and Foundations Division*, vol. 92, no. 5, pp. 51–65, 1966.

[29] S. W. Sloan, "Geotechnical stability analysis," *Géotechnique*, vol. 63, no. 7, pp. 531–571, 2013.